Assessment of Cooling Effect by Urban Park Using a Multi-data Source Approach

Can Trong Nguyen, Amnat Chidthaisong, and Rungnapa Kaewthongrach

Abstract Urban park is a component of urban green infrastructures, essential in urban ecosystems because it delivers various benefits to urban dwellers, from tangible to intangible values. Urban park is widely accepted as a friendly adaptive solution in the context of warmer cities worldwide due to climate change and urbanization impacts. This research quantified the cooling effect of small and medium-sized parks in Bangkok Metropolis and identified primary controlling factors. An integrated approach was adopted to achieve the overarching objectives, including image interpretation from various data sources and Trends-Breakpoints Detection Analysis (TBDA). The research findings revealed that summer's most active cooling distance is around 100–200 meters. When the weather is cooler in winter, the cooling distance expands outward to + 400 and + 1,000 meters depending on park structures and neighboring backgrounds. A park in a region with denser vegetation should have a more moderate cooling effect. Increases in tree areas inside a park and their shape complexity can stimulate the cooling effect, especially in the cooler season. In contrast, the park's water surface only contributes to the cooling effect during the hotter period. The research outcomes are helpful for urban planners in heat mitigation strategies using urban green infrastructures.

Keywords Urban park · Urban green space · Cooling effect · Cooling distance · Park structure

C. T. Nguyen (✉) · A. Chidthaisong
The Joint Graduate School of Energy and Environment, King Mongkut's University of Technology Thonburi, Bangkok 10140, Thailand
e-mail: trongcan.ng@gmail.com

C. T. Nguyen
Faculty of Engineering, Prince of Songkla University (Hatyai Campus), Songkhla 90110, Thailand

C. T. Nguyen · R. Kaewthongrach
Space Technology Research Center, Geo-Informatics and Space Technology Development Agency (GISTDA), Chonburi 20230, Thailand

© The Author(s), under exclusive license to Springer Nature Singapore Pte Ltd. 2024

V. T. Ha et al. (eds.), *Proceedings of the 8th International Conference on Sustainable Urban Development*, Advances in 21st Century Human Settlements,
https://doi.org/10.1007/978-981-99-8003-1_9

1 Introduction

Many studies revealed that Southeast Asia (SEA) cities such as Kuala Lumpur (Malaysia), Bogor (Indonesia), Baguio (Philippines), Yangon (Myanmar), Ho Chi Minh City and Ha Noi (Vietnam), and Bangkok (Thailand) have experienced the warmer trend in land surface temperature (LST) and urban heat islands (UHI), about 0.03 °C to 0.92 °C per year [1, 4, 17, 20, 22, 23, 30]. Higher urban temperature is directly responsible for human thermal comfort and heat-related morbidity and mortality in the city [11, 18]. It also causes pressures on the economy and energy sector for cooling demands, especially during heat waves [16]. Moreover, urban temperature alterations always occur parallel with urbanization, which induces impervious surface extension and narrowing vegetation. These nexuses imply potential solutions for urban design strategies to reduce the harmful impacts of heat exacerbation based on the basic notion of maximizing urban green areas like public parks. In the context of urbanization and escalating climate change, the urban thermal environments are forecasted to be more severe for their inhabitants. Thus, the role of urban green spaces and public parks in mitigating the urban microclimate severity is more prominent and appreciated by managers and urban dwellers.

On the other hand, large parks frequently attract more attention because they are supposed to have diverse and more significant benefits than smaller green spaces. In a crowded city, most land budget is prioritized for residential areas, commercial purposes, and solid urban infrastructures rather than large patches of green spaces [15]. Planning extensive urban forests is challenging in most compact cities. Therefore, we intended to examine the cooling effect of small and medium-sized parks, potentially appropriate for urban greening plans. Additionally, the cooling distance is a principal parameter in the cooling models such as InVEST-Urban Cooling Model [7]. The cooling distance is diverse and fluctuates from park to park depending on many factors. When the cooling distance is specified, the model performance will be significantly improved. The factors controlling the cooling effect will substantially affect a prototype park design to apply to other current and future parks.

This research stands on exploiting diversely free-accessible data to investigate the cooling effect given by the public parks, in which Bangkok metropolis is an empirical study. The controlling elements moderating the cooling effect were then analyzed to identify impacts of the park's structure itself and external environments on the cooling effect, which are helpful information for urban planning toward heat mitigation strategies in the city.

2 Study Sites and Datasets

2.1 Study Sites

Five parks were selected along the urban-periurban gradient of Bangkok metropolis (Thailand), considering their popularity and usable area (Fig. 1). The most extensive park is Chatuchak Botanical Garden which comprises three adjacent parks of Wachira Benchtas, Queen Sirikit, and Chatuchak. Its usable area is about 110 hectares and it has become one of the essential urban green spaces in this compact city. It is followed by Suan Luang Rama IX (shortly Rama 9) with nearly 80 hectares. The following two parks are relatively similar regarding the usable area, Lumpini (57.6 hectares) and Serithai (56 hectares). However, they have significant disparities in location and landscape structures. Lumpini is supposed to be a "green asset" in a cramped neighboring area, while Serithai has its role in rainwater regulation in the periurban of eastern Bangkok. Finally, Thonburirom (*or Thonburi*, 10.058 hectares) is located on the city's west side, which plays a crucial role in aesthetics and its surrounding neighbors' environment.

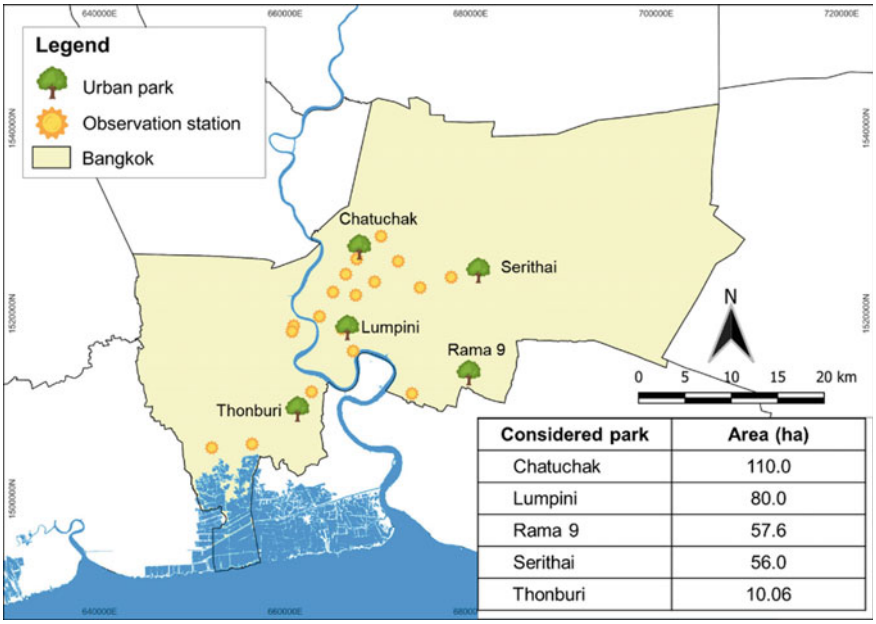

Considered park	Area (ha)
Chatuchak	110.0
Lumpini	80.0
Rama 9	57.6
Serithai	56.0
Thonburi	10.06

Fig. 1 Location of Bangkok, the considered parks, and air quality stations within Bangkok metropolis

2.2 Air Temperature

We obtained air temperature data from the Thailand Pollution Control Department (PCD), which includes 14 stations within the Bangkok metropolitan region. These stations are set up at roadside and ambient locations to hourly measure air temperatures. The temperature at each station was selected based on date and time criteria. In particular, we obtained the air temperature at 10:00 am for analysis because the initial test showed that LST and air temperature reached their highest correlation value at 10:00 am.

2.3 Landsat 8 Imagery

Landsat 8 (OLI/TIRS) surface reflectance is the primary data source to extract surface characteristics and simulate air temperature from these features. The land surface reflectance (LSR) data is atmospherically corrected using Landsat Surface Reflectance Code. The LSR, therefore, minimizes atmospheric influences, especially on temperature data, which is relatively susceptible to atmospheric and cloud conditions. We acquired images under satisfied weather conditions of clear sky or limited clouds covering the study sites and ambient regions. Seven scenes were captured at seven milestones from 2014 to 2016 for training and validating the air temperature predictive model. Whereas the clear-sky images acquired on 19/02/2020, 22/03/2020, and 17/11/2020 were adopted to simulate spatial air temperature for further analyzes in this study.

2.4 Google Earth-Based Imagery

The park's landscapes should be classified by very-high-resolution imagery (VHR) since its scale is frequently small. Yet, we cannot access commercial satellites in this study. Fortunately, Google Earth provides free accessibility to its VHR images at different times. Although Google Earth imagery (GEI) cannot offer diverse spectral information as a standard multispectral image, it can adjust the details to be observed. Thus, the GEI becomes a cost-effective VHR data source widely applied in many urban studies [12, 14]. We collected GEI at each park using the SASPlanet (v200606) tool. The pixel size of the collected GEI is approximately 30 centimeters per pixel edge.

2.5 Sentinel-2 Imagery

GEI is relatively approriate for mapping in detail land cover in a small-scale area. However, it shows limitations in a larger region when the detail of GEI becomes its drawbacks in terms of processing performance. More explicitly, there are potential noises from building shadows, colors of different roof materials, tree canopy structures, and even water surface waves. Therefore, we adopted moderate-high spatial resolution satellite imagery of Sentinel-2 (10 meters) to classify landscape information around the park from its border to 2 km. Sentinel-2 L2A images were collected with an acquisition strategy of the smallest difference in captured date of Landsat-8 images above. Two scenes were downloaded directly from the Sentinel Hub on 21/02/2020 (10:37) and 29/08/2020 (10:35). These images have a low cloud coverage rate of 0.47% and 5.81% for the image in February and August, respectively.

3 Methodology

3.1 Land Cover of the Park and Surrounding Areas

Landscapes of the parks were classified using Google Earth imagery. It comprises five land cover categories of wood tree, grassland, soil/pavement, buildings, and lake/pond. Firstly, the acquired images were reprojected before they were analyzed by object-oriented classification. The images were then overcome through a segmentation procedure, which groups nearby similar pixels together based on their similarities in spectral information, proximity, pattern, and so on. Segment Mean Shift (SMS) technique was adopted to analyze the GEI. Subsequently, the segmented images were classified by the ISODATA (Iterative Self-Organizing Data Analysis) unsupervised classifier. To cluster pixels into N user-defined groups, the algorithm randomly sets cluster centers and assigns pixels to clusters using minimum distance. The clusters will be merged or split based on the minimum distance among the cluster's centers. The progress is repeated until all pixels are precisely separated and the number of clusters reaches the user-defined number. In this study, the initial clusters of $N = 30$ were set for classification. The subclusters were combined altogether if they presented an identical land cover type when collated with image visualization.

The neighboring regions of each park were extracted by multispectral imagery of Sentinel-2, which grouped into major land cover categories such as impervious surfaces, vegetation, water bodies, and bare land. First, the multispectral bands (i.e., visible wavelength, Red-Edge, NIR, and SWIR) were consistently resampled pixel size of 10 meters. After that, we applied integration of principal component analysis (PCA) and ISODATA unsupervised classifier to retrieve the park's neighboring land cover. The initial cluster number was $N = 15$ because Sentinel-2 imagery is less detailed than GEI. Finally, the classified images were combined to generate a map based on general land cover types.

3.2 Air Temperature Estimation Using Machine Learning

Surface characteristics extraction. The surface characteristics were described by spectral indices, representing three primary land cover patterns of vegetation, impervious surfaces, and water bodies. Particularly, vegetation was depicted by the Normalized Difference Vegetation Index (NDVI) and Enhanced Vegetation Index (EVI). NDVI is a well-known index to identify live green foliage relating to photosynthetically active radiation (PAR) and Near Infrared (NIR) light [9, 24]. However, it shows limitations when vegetation becomes denser. EVI was proposed to overcome the NDVI limitations by adjusting the NDVI formula by blue light and constants [10]. Hence, we also obtained EVI to separate different vegetation canopies, which are expected to influence the air temperature. The next crucial land cover type is urban features, which mainly contribute to urban warming due to the thermal characteristics of urban materials. Therefore, we calculated two urban indices (i.e., Urban Index (UI) and Normalized Difference Built-up Index (NDBI)) to test which index better performs for air temperature estimation. Finally, the water surfaces were defined by the Modified Normalized Difference Water Index (MNDWI) – an optimal water index to locate water features in urban areas [28].

Land surface temperature retrieval. Land surface temperature (LST) was retrieved using a widely applied algorithm, which converts DNs values to LST by calibrating brightness temperature (T_B) using NVDI-based land surface emissivity (LSE) (Eq. 3) [3, 25, 27]. Firstly, vegetation fraction (FVC) was calculated by calibrating specific NDVI pixels by NDVI values of fully dense vegetation ($NDVI_V$) and completely bare soil surface ($NDVI_S$) (Eq. 1) (Carlson & Ripley, 1997). Then, LSE was estimated by an empirical equation using FVC for Landsat OLI/TIRs (Eq. 2) [21, 26].

$$FVC = ((NDVI - NDVI_S) / (NDVI_V - NDVI_S))^2 \quad (1)$$

$$\varepsilon = 0.00149 \times FVC + 0.985481 \quad (2)$$

$$T_S = (T_B/(1 + (\lambda T_B/\rho) \ln \varepsilon)) - 273.15 \quad (3)$$

where FVC is vegetation fraction; $NDVI_S$ and $NDVI_V$ are vegetation index of fully dense vegetation and bare soil, respectively; ε is land surface emissivity for Landsat OLI; TS the is the land surface temperature (°C); TB is brightness temperature in Kelvin; λ is the wavelength of emitted radiance (i.e., Landsat OLI is band 10, λ_{B10} = 10.89 μm); $\rho = hc/\sigma$, with $\rho = 1.438 \times 10^{-2}$ Mk.

Optimal distance determination. Air temperature at a particular location is regulated by its surrounding landscape rather than its land cover. Therefore, we should determine which distance that land cover mainly drives air temperature variations. Firstly, aggregated images of surface indices were generated with the number of pixels on each edge that belongs to an odd number subset, $F = \{3,5,7,\ldots, 65,67\}$.

These pixels correspond to distances from 90 to 2,100 meters from the stations. Next, the index values were extracted and compared to air temperature at 10:00 a.m. using the Pearson correlation coefficient. The distance of each index was noted when the correlation coefficient achieved the first highest value. The influential distance was subsequently determined as a general distance throughout all indicators. The effective distance is 750 meters based on our initial test.

Air temperature predictive model. LST is a critical variable in air temperature prediction models because it has the most significant relationship with other surface indicators [8, 19]. The best model was detected through a model performance test using cross-validation. Specifically, the simple model of only LST, its combination with each surface indicator, and two other Random Forest (RF) synthetic models were evaluated with iteration $N = 1000$. The most optimal model is determined when a model achieves a higher accuracy with fewer predictors. Finally, the optimally predictive model was applied to its contributors of spatial surface elements to simulate air temperature in entire study areas.

3.3 Analyzing Climate Regulation Effect

The influential distance of the park was analyzed by trend and breakpoint detection analysis using the greenbrown R package [5]. Theoretically, the greenbrown is performed on time series data to explore how the land phenology changes. This study assumed that air temperature variation every 100 meters until 2,100 meters is a node in time series data. As a result, the influential distance was detected at a breakpoint where air temperature significantly drops from the park site.

In addition to the land use, land cover (LULC) area, the landscape metrics, including Percentage of Landscape (PLAND), Aggregation Index (AI), and Landscape shape index (LSI), were computed for park structures and surrounding areas for each 100-m buffer zone [13]. Subsequently, we analyzed the correlation between air temperature difference (i.e., the gaps between near park zones and highly dense urban areas) and each landscape metric using the Pearson correlation coefficient.

4 Results and Discussions

4.1 Park's Land Cover Structure

Landscapes of the considered parks interpreted from GEI are shown in Fig. 2. Unlike the classic parks only occupied by vegetation and woodlands, these parks incorporate diverse landscapes of wood trees, lawns, and water surfaces (Fig. 2). These designs are based on modern design perspectives to provide diverse sceneries and take their environmental advantages. In addition to the difference in usable area, their structures

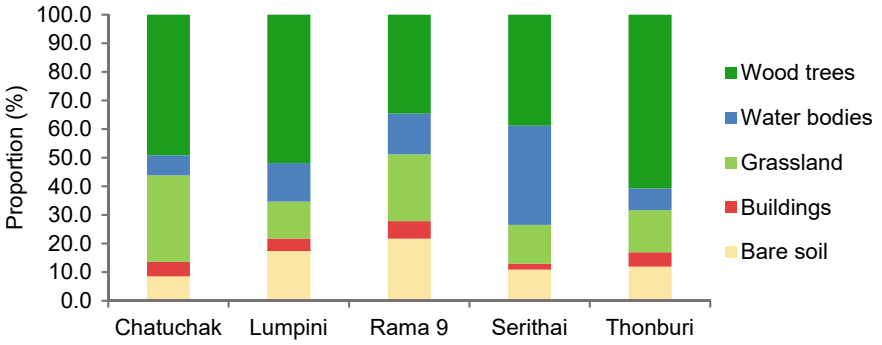

Fig. 2 Landscape proportion in the considered parks delineated from GEI

are relatively diverse. The pivotal object throughout the parks is vegetation, i.e., it is contributed by any green patch. The woodland proportion always maintains from 38.8% (Serithai) to 60.7% (Thonburi) (Fig. 2). Lumpini and Chatuchak also hold a relatively large area of the woodland, about 51.9% and 49.2%, respectively. Chatuchak Park uses 30.3% of the space for expansive lawns, the most extended lawn area among the parks. Regarding the contribution of water surfaces in the parks, Serithai is highlighted with a central lake, where the water surface area rate is up to 34.7%.

4.2 Spatial Air Temperature

The optimal distance for air temperature simulation was 750 meters. The influential distance was utilized as a buffer distance to extract surface indicators for model testing. Model accuracy for different RF-model combinations is shown in Table 1. Notably, the model with solely LST achieves relatively high accuracy, 0.91 ± 0.028. Adding one or more auxiliary data of surface indicators improves the accuracy of air temperature simulation. Among vegetation indices, the model contributed by EVI is more efficient than the NDVI model, with an accuracy is 0.94 versus 0.93, respectively. The models of the urban index are not much different in performance assessed by mean accuracy; nevertheless, the UI model reaches higher maximum accuracy implying potential efficiency compared to NDBI. The model with MNDWI contribution also obtained 0.94 ± 0.02. According to these analyzes, we proposed and tested an optimal model (M7), constituted by the favorable elements (i.e., LST, EVI, UI, and MNDWI). Its performance reached a high level of 0.96 ± 0.014 against the above models, with the highest value even achieved at 0.98. The model performance of all elements (M8) is not much distinctive from the M7 model, while the M7 model can simulate air temperature with fewer variables. As a result, the M7

Table 1 The accuracy obtained by cross-validation from different RF-model combinations

Model	Predictors	Average Accuracy	Std.
M1	LST	0.906	0.0285
M2	LST, NDBI	0.941	0.0185
M3	LST, EVI	0.932	0.0225
M4	LST, UI	0.942	0.0187
M5	LST, NDVI	0.924	0.0273
M6	LST, MNDWI	0.936	0.0208
M7	LST, EVI, UI, MNDWI	0.954	0.0150
M8	LST, NDBI, UI, NDVI, EVI, MNDWI	0.958	0.0136

model was considered as an ideal model for spatial air temperature estimation in Bangkok metropolis, $R^2 = 0.91$ and $RMSE = 0.89$. The spatial simulation for air temperature entirely in Bangkok on free cloud dates of 19/02/2020, 22/03/2020, and 17/11/2020 was obtained by applying the ideal M7 model.

4.3 Spatiotemporal Distinctness in Cooling Effect Distance

The average Ta within the park boundary extracted from the estimated air temperature is shown in Table 2. Overall, the park's air temperature increases from February to March; in November, it drops to values less than that in February. The highest temperatures throughout the months are at Chatuchak Park, while the lowest temperatures are held by Thonburirom Park (February and November) and Serithai (November). For example, we consider temperature variations between February and March, which shows that the most easily variated parks are Lumpini (ΔTa = 2.29 °C) and Thonburirom (ΔTa = 2.14 °C). On the contrary, Serithai and Rama 9 tend to be more stable in temperatures over time, especially Serithai ΔTa = 0.55 °C.

We investigated the cooling effect of each park using breakpoint analysis (Fig. 3). Firstly, the Ta value changes along the horizonal buffer zones from 0 to 2000 meters were assumed and analyzed as annual time series data. Then, the trend and breakpoints were tested to determine the statistically significant trends and breakpoints.

Table 2 Each park's average air temperature (°C) in February, March, and November 2020

Park	February	March	November
Chatuchak	27.678 ± 0.971	29.561 ± 0.879	27.417 ± 1.064
Lumpini	26.893 ± 0.166	29.180 ± 0.367	26.617 ± 0.496
Rama 9	27.087 ± 0.139	28.352 ± 0.522	26.577 ± 0.257
Serithai	27.659 ± 0.252	28.205 ± 0.487	27.989 ± 0.248
Thonburi	26.372 ± 0.035	28.513 ± 0.352	25.283 ± 0.001

The principles accepted for this analysis is the temperature at the park, which is controlled by cooling features such as wood trees, lawns, and water surfaces, being coolest in comparison to surrounding impervious surfaces; plus, the temperature gradually increases under the influences of dense urban areas until the temperature drops again when it reaches rural areas with extensive cooler surfaces and landscapes.

Chatuchak can control the air temperature around the park by about 600 ± 100 meters in November. The influential distance is narrowed from February to March, approximately 200 ± 100 meters (i.e., it can cool up to 400 meters) and 200 ± 100 meters. The Lumpini Park can also cool down its neighboring areas up to 600 ± 100 meters in winter. Yet, this distance is solely 200 meters in February.

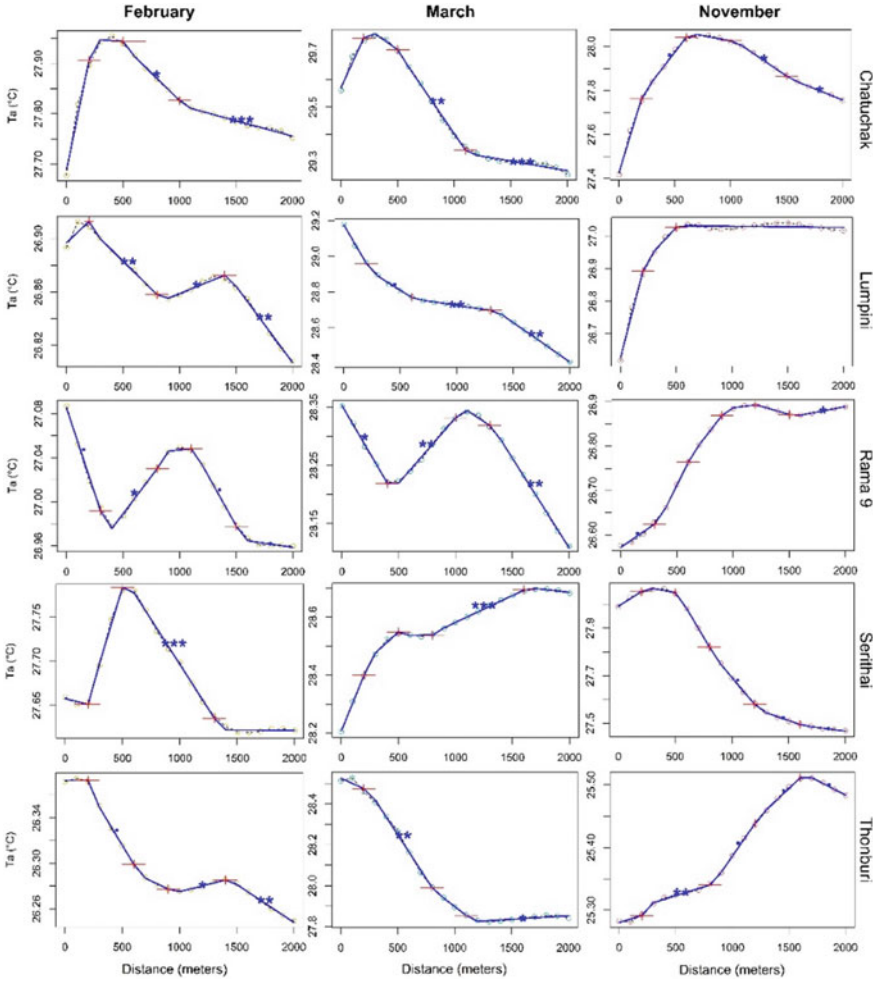

Fig. 3 Air temperature changes along the horizontal transect and corresponding changepoints (red nodes)

In the mid-summer, Lumpini Park does not show a cooling effect anymore to its surrounding areas.

Surprisingly, the biggest park of Rama 9 Park has no significant cooling effect through the analysis for both February and March. The cooling effect, however, significantly improves in the winter season. The areas around the park, about 900 ± 100 meters, are primarily affected, and the active distance can expand up to 1,200 meters. In Serithai Park, only the areas adjacent to the park (about 100 meters) can receive the cooling effect. The affected regions enlarged by 200 meters in November.

In contrast to other parks, i.e., the cooling effect weakens in the mid-summer, the Serithai Park shows a remarkable regulative capacity of 500 ± 100 meters. On the other hand, the smallest park of Thonburirom Park can reduce the air temperature by around 200 meters and 100 meters in February and March. However, these distances are insignificant. During the winter season, the active cooling distance achieves 1,600 ± 100 meters, the most extended distance among the considered parks in Bangkok.

4.4 Pivotal Factors Regulate Park Cooling Effect

The park's cooling effect fluctuates throughout the year depending on seasons, while its inside structures and surrounding environments remain relatively stable as a kind of evergreen vegetation. Our analyzes for air temperature variations within 100 meters and 500 meters, 100 meters represent a location cooled down by the park, and 500 meters is a place of denser urban areas (Fig. 4), revealing the parks' temperature and their cooling magnitude are closely associated with location and park structures. For instance, the temperature gap between the two mentioned locations in November (i.e., when all parks' cooling capacities tend to be consistent and clarified) decreases gradually in Chatuchak (0.367 °C), Lumpini (0.244 °C), Rama 9 (0.13 °C), Thonburi (0.042 °C), and Serithai (0.016 °C). The more significant the temperature gap, the more influential the park with a high cooling effect is. It means that Chatuchak and Lumpini have a higher cooling effect than other parks.

Figure 4 shows the background of the parks where they are located. Regarding urban density from 500 meters outwards, Chatuchak and Lumpini stand within the metropolitan areas with the urban proportion exceeding 50% from 300 meters. Similarly, Serithai and Thonburi are determined to be in periurban areas as the urban densities fluctuate around a threshold of 50%. Rama 9 is a suburban park since its surrounding urban density is approximately 35% within the first 1,500 meters from the park boundary. The correlation analysis of the park's neighboring areas influences the park's temperatures and cooling effect. The results concede that the park's cooling effect is assisted by outside vegetation. Increasing the shape complexity of vegetation patches and green areas is the most influential factor. In contrast, the cooling effect is weakened by increasing impervious surfaces.

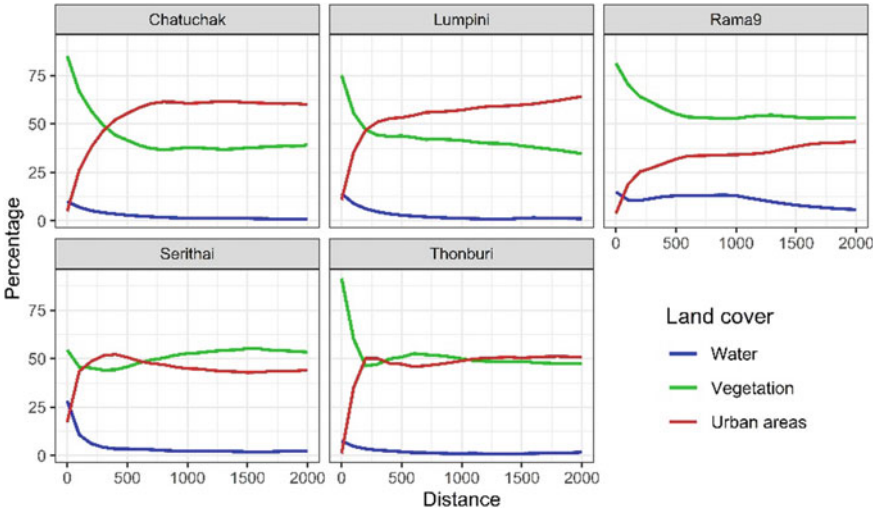

Fig. 4 Proportion of LULC from the park boundary outwards to neighboring areas

Regarding the park itself structures, it tends to be more influential in the cooling effect. The tree area is the most statistically significant element controlling cooling intensity ($R = 0.97$, $P < 0.01$). Moreover, the tree arrangement, i.e., green patches, are planted closely together into plates of complex shapes, which also governs to cool down park's neighboring areas. Besides, the water surface area inside the park in the form of a lake and wetland helps to improve the cooling effect outside the park.

The correlation analysis between the park characteristics, background patterns, and cooling intensity is shown in Fig. 5. The results indicate that both the outside and inside environments drive the cooling effect. In particular, the relationships are more significant in November against February and March. Outside vegetation substantially influences park cooling intensity, with an increase in vegetation proportion (PLAND) and its assembly into big patches (AI, LPI) being the most important determinants. In contrast, the compact impervious surfaces are represented by the spatial metrics of area, proportion, and aggregation, significantly weakening those effects encouraged by green spaces. Regarding the park's structures, the tree area is the most statistically significant factor influencing cooling intensity, notably in November ($R = 0.97$, $P \leq 0.01$). However, the influence is moderate in February and even non-existent in March. The tree arrangement, i.e., green patches, are planted tightly together to form plates of close and complicated shapes (i.e., AI and LSI), which also cools the park's surrounding regions. Furthermore, the park's water surface area, such as the lake and marsh, aids in improving the cooling effect outside the park, particularly during the hot season.

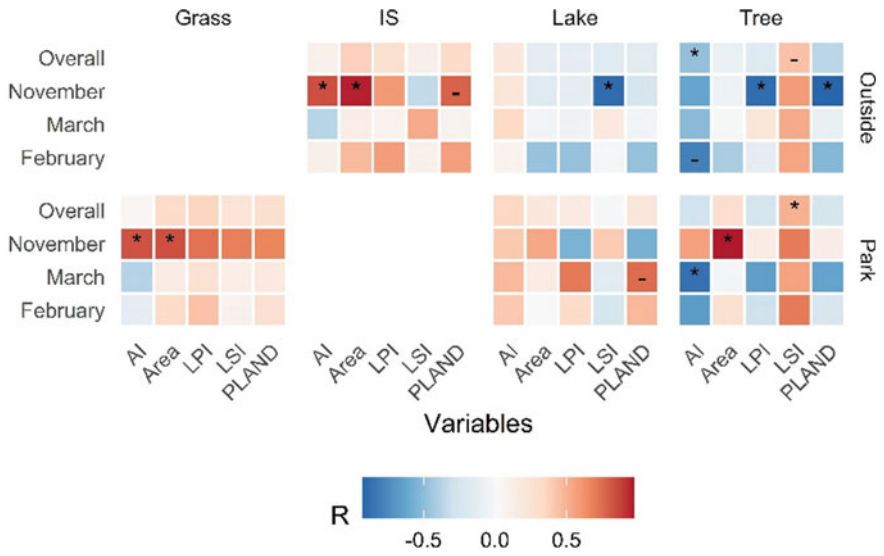

Fig. 5 Heatmap shows correlation coefficients between cooling effect and landscape metrics. Note: Symbols (*) and (-) indicate significance levels at $\leq 5\%$ and ~ 10%. Grass: grassland; IS: impervious surfaces such as built-up, pavements, and roads; Lake: water surfaces; Tree: vegetation and woodland inside and outside the parks

4.5 Implications for Urban Environment and Planning

The considered parks in this study are ranked from small to medium size (10–110 hectares). Yet, the active cooling distance is smaller than about one-third of a 150-hectare park (200–300 meters) [6] and six times that of a 680-hectare large park (~1400 meters) [29]. Therefore, in urban green space design, small and medium-sized parks placed at the most beneficial distance from each other should be emphasized to maximize the limited urban land budget while ensuring open space accessibility for all inhabitants. Furthermore, a reasonable distribution of parks with other green infrastructures outside the parks disperses the concentrated pressures, improving the cooling effect.

Heat reduction is supported by combining blue and green spaces. Timber trees should be the primary focus. However, the water surface is also a supportive element. The integrated blue spaces (e.g., a tree-shaded lake and artificial wetland with appropriate aquatic plants) should be applied instead of the monotonic and extensive lake in urban planning. A lawn serves as a venue for outdoor leisure, such as picnics, assemblies, group activities, and a place to set up exercise equipments. At the same time, a cluster of wood trees significantly decreases air temperature. To minimize monotonic landscapes, the proportions of wood trees, lawns, and lakes within a park should be adjusted appropriately. In addition, the arrangement of trees should be

considered, with individual trees being replaced with clusters of trees with intricate forms and edges to increase the cooling effect.

Though landscape integration is essential to enrich urban biodiversity and exploit different and beneficial angles, the water surface's cooling effect is prominent in hot weather [30]. The effect is reduced at nighttime due to heat release, especially for polluted water in the city. Therefore, in park design, the ratios of vegetated surfaces to water surfaces should be insightfully considered to diversify landscapes and optimize the cooling impact over time.

5 Conclusion

The cooling effect of public parks and the elements that influenced it were investigated. Using multiple data sources, we found the integrated landscapes in all parks with a high share of green and blue areas at various combinative ratios. Aside from that, there are differences in cooling distance, which vary according to the season. During the summer, the active cooling distance is usually between 100 and 200 meters. However, the cooling distance extends outward 400 meters and up to 1,000 meters, depending on park structures and the surrounding background. The tree area inside the park and the arrangement of green space patches are the most critical factors controlling climate regulation. Although the other neighboring elements are insignificant in statistics, they are worthily considered in urban planning strategies to mitigate urban heat islands, such as low urban density, high vegetation area, and vegetation shape complexity. Furthermore, the water surface provides an unsteady cooling effect both within and outside the park. As a result, using water surfaces as part of a heat mitigation plan should be carefully examined to achieve a more appropriate and sustainable strategy for urban heat reduction.

Acknowledgements This work was supported by the Petchra Pra Jom Klao scholarship of the King Mongkut's University of Technology Thonburi (no. 09/2562). We would like to show our gratitude to all the agencies that provided data for this study, including the Thailand Department of Pollution Control (PCD), United States Geological Survey (USGS), European Space Agency (ESA), and Google Earth.

References

1. Amanollahi J, Tzanis C, Firuz M, Makmom A (2016) Urban heat evolution in a tropical area utilizing Landsat imagery. Atmos Res 167:175–182. https://doi.org/10.1016/j.atmosres.2015.07.019
2. Carlson TC, Ripleya D (1997) On the relationship between NDVI, fractional vegetation cover, and leaf area index. Remote Sens Environ 62:241–252. https://doi.org/10.1016/S0034-4257(97)00104-1

3. Estoque RC, Murayama Y (2016) Quantifying landscape pattern and ecosystem service value changes in four rapidly urbanizing hill stations of Southeast Asia. Landscape Ecol 31(7), 1481–1507. https://doi.org/10.1007/s10980-016-0341-6
4. Estoque RC, Murayama Y (2017) Monitoring surface urban heat island formation in a tropical mountain city using Landsat data (1987–2015). ISPRS J Photogramm Remote Sens 133:18–29. https://doi.org/10.1016/j.isprsjprs.2017.09.008
5. Forkel M, Carvalhais N, Verbesselt J, Mahecha MD, Neigh CSR, Reichstein M (2013) Trend Change detection in NDVI time series: Effects of inter-annual variability and methodology. Remote Sensing 5(5):2113–2144. https://doi.org/10.3390/rs5052113
6. Hamada S, Ohta T (2010) Urban Forestry & Urban Greening Seasonal variations in the cooling effect of urban green areas on surrounding urban areas. Urban Forestry & Urban Greening 9(1):15–24. https://doi.org/10.1016/j.ufug.2009.10.002
7. Hamel P, Guerry AD, Polasky S, Han B, Douglass JA, Hamann M, Janke B, Kuiper JJ, Levrel H, Liu H, Lonsdorf E, McDonald RI, Nootenboom C, Ouyang Z, Remme RP, Sharp RP, Tardieu L, Viguié V, Xu D, Daily GC (2021) Mapping the benefits of nature in cities with the InVEST software. NPJ Urban Sustainability, 1(1). https://doi.org/10.1038/s42949-021-00027-9
8. Hereher ME, El Kenawy A (2020) Extrapolation of daily air temperatures of Egypt from MODIS LST data. Geocarto Int 0(0), 1–17. https://doi.org/10.1080/10106049.2020.1713229
9. Karnieli A, Bayasgalan M, Bayarjargal Y, Agam N, Khudulmur S, Tucker CJ (2006) Comments on the use of the Vegetation Health Index over Mongolia. Int J Remote Sens 27(10):2017–2024. https://doi.org/10.1080/01431160500121727
10. Liu HQ, Huete A (1995) Feedback based modification of the NDVI to minimize canopy background and atmospheric noise. IEEE Trans Geosci Remote Sens 33(2):457–465. https://doi.org/10.1109/36.377946
11. Lowe SA (2016) An energy and mortality impact assessment of the urban heat island in the US. Environ Impact Assess Rev 56:139–144. https://doi.org/10.1016/j.eiar.2015.10.004
12. Malarvizhi K, Kumar SV, Porchelvan P (2016) Use of High Resolution Google Earth Satellite Imagery in Landuse Map Preparation for Urban Related Applications. Procedia Technol 24:1835–1842. https://doi.org/10.1016/j.protcy.2016.05.231
13. McGarigal K, Cushman SA, Ene E (2012) FRAGSTATS v4: spatial pattern analysis program for categorical and continuous maps. Computer software program produced by the authors at the University of Massachusetts
14. Mering C, Baro J, Upegui E (2010) Retrieving urban areas on Google earth images: Application to towns of West Africa. Int J Remote Sens 31(22):5867–5877. https://doi.org/10.1080/01431161.2010.512311
15. Nguyen CT, Chidthaisong A (2022) Urban Green Space Inventory using Different Spatial Resolution Satellite Images: Practical notes in Bangkok. The 11th International Conference on Environmental Engineering, Science and Management (pp. 333–340). Environmental Engineering Association of Thailand (EEAT)
16. Nguyen CT, Diep NTH, Diem PK (2021) Factors affecting urban electricity consumption: a case study in the Bangkok Metropolitan Area using an integrated approach of earth observation data and data analysis. Environ Sci Pollut Res 28:12056–12066. https://doi.org/10.1007/s11356-020-09157-6
17. Nurwanda A, Honjo T (2019) The Prediction of City Expansion and Land Surface Temperature in Bogor City, Indonesia. Sustainable Cities and Society, 52(2020). https://doi.org/10.1016/j.scs.2019.101772
18. Santamouris M (2020) Recent progress on urban overheating and heat island research. Integrated assessment of the energy, environmental, vulnerability and health impact. Synergies with the global climate change. Energy and Buildings, 207, 109482. https://doi.org/10.1016/j.enbuild.2019.109482
19. Sohrabinia M, Zawar-Reza P, Rack W (2015) Spatio-temporal analysis of the relationship between LST from MODIS and air temperature in New Zealand. Theoret Appl Climatol 119(3–4):567–583. https://doi.org/10.1007/s00704-014-1106-2

20. Son NT, Chen C, Chen C, Thanh B, Vuong TH (2017) Assessment of urbanization and urban heat islands in Ho Chi Minh City, Vietnam using Landsat data. Sustain Cities Soc 30:150–161. https://doi.org/10.1016/j.scs.2017.01.009
21. Son NT, Thanh BX (2018) Decadal assessment of urban sprawl and its effects on local temperature using Landsat data in Cantho city. Vietnam. Sustainable Cities and Society 36(2018):81–91. https://doi.org/10.1016/j.scs.2017.10.010
22. Srivanit M, Hokao K (2012) Thermal Infrared Remote Sensing for Urban Climate and Environmental Studies: An Application for the City of Bangkok, Thailand. Journal of Architectural/Planning Research and Studies 9(1):83–100
23. Tran DX, Pla F, Latorre-Carmona P, Myint SW, Caetano M, Kieu HV (2017) Characterizing the relationship between land use land cover change and land surface temperature. ISPRS J Photogramm Remote Sens 124:119–132. https://doi.org/10.1016/j.isprsjprs.2017.01.001
24. Tucker CJ (1979) Red and photographic infrared linear combinations for monitoring vegetation. Remote Sens Environ 8(2):127–150. https://doi.org/10.1016/0034-4257(79)90013-0
25. USGS (2016) Landsat 8 (L8) Data Users Handbook (LSDS-1574 version 2.0). In USGS Landsat User Services. U.S. Geological Survey
26. Van De Griend AA, Owe M (1993) On the relationship between thermal emissivity and the normalized difference vegetation index for natural surfaces. Int J Remote Sens 14(6):1119–1131. https://doi.org/10.1080/01431169308904400
27. Weng Q, Lu D, Schubring J (2004) Estimation of land surface temperature-vegetation abundance relationship for urban heat island studies. Remote Sens Environ 89(4):467–483. https://doi.org/10.1016/j.rse.2003.11.005
28. Xu H (2006) Modification of normalised difference water index (NDWI) to enhance open water features in remotely sensed imagery. Int J Remote Sens 27(14):3025–3033. https://doi.org/10.1080/01431160600589179
29. Yan H, Wu F, Dong L (2018) Influence of a large urban park on the local urban thermal environment. Sci Total Environ 622–623:882–891. https://doi.org/10.1016/j.scitotenv.2017.11.327
30. Yi WC, Hu BKH, Myint SW, Feng CC, Chow WTL, Passy PF (2018) Patterns of land change and their potential impacts on land surface temperature change in Yangon, Myanmar. Sci Total Environ 643:738–750. https://doi.org/10.1016/j.scitotenv.2018.06.209